ELSEVIER

Nuclear Physics A 588 (1995) 667–692

NUCLEAR PHYSICS A

Probing the ground-state and transition densities of halo nuclei

C.A. Bertulani [a,1], H. Sagawa [b]

[a] *Gesellschaft für Schwerionenforschung, KPII, Planckstr. 1, D-64291 Darmstadt, Germany*
[b] *Center for Mathematical Sciences, University of Aizu, Ikki-Machi, Aizu-Wakamatsu, Fukushima 965, Japan*

Received 20 December 1994; revised 26 January 1995

Abstract

We investigate the use of elastic and inelastic scatterings with secondary beams of radioactive nuclei as a means to obtain information on ground-state densities and transition matrix elements to continuum states. An eikonal model is developed for this purpose by using the folding potential. In particular we discuss possible signatures of halo wavefunctions in elastic- and inelastic-scattering experiments.

1. Introduction

Reactions with radioactive beams are a useful tool to understand the properties of nuclei far from the stability line (see, e.g., Ref. [1]). Up to the present these reactions are mainly restricted to studies of reaction cross sections and momentum distributions of the fragments [2,3]. Elastic scattering has been studied in several experiments [4–8]. Inelastic scattering has also been studied, but very few experiments for Coulomb-breakup processes only [9,10] are available so far. Usual techniques with stable nuclei, like photo-nuclear absorption and electron scattering are far beyond the present experimental possibilities. The study of reaction cross sections, momentum distributions, and elastic scattering gives us a very limited access to the information on the internal structure of exotic nuclei, although many intriguing properties of these nuclei have been deduced in these experiments. An example is the discovery of the extended matter distribution in very light neutron-rich nuclei, the so-called halo nuclei [2].

The study of inelastic-excitation cross sections is the natural step to increase our knowledge on the nuclei far from the stability line. In fact, Coulomb and nuclear

[1] Present address: Instituto de Física, UFRJ, 21945-970 Rio de Janeiro, Brazil.

Elsevier Science B.V.
SSDI 0375-9474(95)00022-4

excitations in nucleus–nucleus scattering are well-established tools for the spectroscopy of stable nuclei and are complementary to photo-nuclear and electron-scattering experiments. Due to the low luminosity of radioactive nuclear beams, experiments are possible only when the cross sections are sufficiently large. For inelastic scattering this is the case for the Coulomb excitation of loosely bound nuclei, e.g., ^{11}Li and ^{11}Be, incident on heavy targets [9,10]. The beams of exotic nuclei are often available at intermediate and high energies, $E_{\rm lab} > 50$ MeV/nucleon [1]. At these energies the Coulomb field favors the dipole excitations. On the other hand, the nuclear interaction favors the monopole and quadrupole excitations.

A study of nuclear excitations of the halo nucleus ^{11}Li has been done in Ref. [11]. It was shown that the excitations of low-lying continuum states of ^{11}Li have substantial cross sections and they can reach some 100 mb/sr at forward angles. In this article we extend the model of Ref. [11] to include Coulomb-excitation processes. Inelastic-excitation processes are unavoidably accompanied by elastic scattering. We thus also make a study of elastic-scattering processes with unstable nuclei. Under simplifying assumptions, which we try to justify in the next sections, elastic scattering allows one to get information on the ground-state properties of the exotic nuclei, while the inelastic-scattering processes tell us about the transition densities for the excitation. If the ground-state wavefunction can be deduced from the elastic scattering, the excited-state wavefunctions can be inferred from the inelastic-excitation processes.

The extraction of the above-mentioned information from the experimental data suffers from several difficulties which arise due to the complexity of the reaction mechanism. The ideal situation occurs when the reaction mechanism can be explained with very simple models. In this article we use a simple and tractable model for the reaction mechanisms and apply it to the study of the scattering of unstable beams. Under some circumstances it is shown that our model can be very useful to extract the ground-state properties of exotic nuclei. A study of this feature is presented in Sections 3 and 4. A brief explanation of the calculation of ground-state densities for exotic nuclei is given in Section 3. These densities are used as inputs in the calculation of the elastic cross sections, which are compared to some available experimental data in Section 4. To show the feasibility of the models used, we also compare the theoretical predictions with some experimental data for reactions with stable nuclei.

The inelastic-scattering cross sections are discussed in Sections 5 and 6. In Section 5 we deduce formulas using the deformed-potential model and folding model for inelastic excitations. The equations for the folding model have been used in Ref. [11]. We also present appropriate formulas for the case of Coulomb excitation. These equations are applied in Section 6 to discuss the angular distributions for inelastic processes with stable and unstable nuclear beams. In Section 7 we present our conclusions.

2. Elastic scattering

The elastic scattering in nucleus–nucleus collisions is a well-established tool for the investigation of ground-state densities. This is because the optical potential can be

related to the ground-state densities by means of a folding of the nucleon–nucleon interaction with the nuclear densities of two colliding nuclei. But, this relationship is not quite straightforward. It depends on the effective interaction used, a proper treatment of polarization effects, and so on (for a review see, e.g., Ref. [12]). At higher bombarding energies than $E_{\rm lab} \sim 50$ MeV/nucleon, a direct relationship between the nuclear densities and the optical potential is possible, as long as the effects of multiple nucleon–nucleon scattering can be neglected. The effects of real, or virtual, nuclear excitations are small since the excitation energies involved are much smaller than the bombarding energies. Lenzi, Vitturi and Zardi [13] have performed an extensive study of the nuclear scattering of stable nuclei at high energies. From their study one concludes that a simple relationship between the ground-state densities and the elastic-scattering cross sections quite often yields very reasonable results, as compared to the experiments. We adopt here a similar approach and extend it to study the scattering of exotic nuclei.

At high energies the elastic-scattering cross section for proton–nucleus collisions is well described by means of the eikonal approximation [14]. The optical potential for proton–nucleus scattering is assumed to be of the form

$$U(r) = U_0(r) + U_S(r)(\boldsymbol{L}\cdot\boldsymbol{S}) + U_C(r), \tag{1}$$

where

$$U_0(r) = V_R f_R(r) - iW_V f_I(r) + 4ia_I W_I \frac{d}{dr} f_I(r) \tag{2}$$

and

$$U_S(r) = 2\left(\frac{\hbar}{m_\pi c}\right)^2 V_S \frac{1}{r}\frac{d}{dr} f_S(r) \tag{3}$$

are the central and spin–orbit part of the potential, respectively, and $U_C(r)$ is the proton–nucleus Coulomb potential. The Fermi functions f_i are given by

$$f_i(r) = \left[1 + \exp\left(\frac{r - R_i}{a_i}\right)\right]^{-1}, \tag{4}$$

with $R_i = r_i A^{1/3}$.

In the eikonal approximation, the proton–nucleus elastic-scattering cross section is given by [14]

$$\frac{d\sigma_{\rm el}}{d\Omega} = |F(\theta)|^2 + |G(\theta)|^2, \tag{5}$$

where

$$F(\theta) = f_C(\theta) + ik\int_0^\infty db\, bJ_0(qb)\, \exp[i\chi_C(b)] \times\{1 - \exp[i\chi_0(b)]\, \cos[kb\chi_S(b)]\} \tag{6}$$

and

$$G(\theta) = ik\int_0^\infty db\, bJ_1(qb)\, \exp[i\chi_C(b) + i\chi_0(b)]\, \sin[kb\chi_S(b)]. \tag{7}$$

In the equation above $q = 2k \sin(\theta/2)$, where θ is the scattering angle, J_0 (J_1) is the zero (first) order Bessel function. The eikonal phase $\chi_{0(S)}$ is given by

$$\chi_{0(S)}(\boldsymbol{b}) = -\frac{1}{\hbar v}\int_{-\infty}^{\infty} U_{0(S)}(\boldsymbol{b}, z)\, dz. \tag{8}$$

For the Coulomb eikonal phase we use the approximation, valid for a point nucleus,

$$\chi_C(b) = \eta \ln(kb) \quad \text{with} \quad \eta = \frac{2Z_1Z_2e^2}{\hbar v}, \tag{9}$$

where Z_1 and Z_2 are the proton ($Z_1 = 1$) and the nuclear charges, respectively. The Coulomb phase will be changed for a finite-charge distribution of the nucleus [15]. For example, assuming a uniform charge distribution with radius R the Coulomb phase becomes

$$\chi_C(b) = \eta\left\{\Theta(b-R)\ln(kb) + \Theta(R-b)\left[\ln(kR) + \ln\left(1+\sqrt{1-\frac{b^2}{R^2}}\right)\right.\right.$$
$$\left.\left. - \sqrt{1-\frac{b^2}{R^2}} - \tfrac{1}{3}\left(1-\frac{b^2}{R^2}\right)^{3/2}\right]\right\}, \tag{10}$$

where Θ is the step function. This expression is finite for $b = 0$, contrary to Eq. (9). If one assumes a gaussian distribution of charge with radius R, appropriate for light nuclei, the Coulomb phase becomes

$$\chi_C(b) = \eta\left[\ln(kb) + \tfrac{1}{2}E_1\left(\frac{b^2}{R^2}\right)\right], \tag{11}$$

where the error function E_1 is defined as

$$E_1(x) = \int_x^{\infty} \frac{e^{-t}}{t}\, dt. \tag{12}$$

This phase also converges, as $b \to 0$.

We have noticed in our numerical calculations that the above corrections to the approximation (9) do not modify the calculated cross sections appreciably. Moreover, one can show that in the eikonal approximation, the phase defined in Eq. (9) yields exactly the Coulomb-scattering amplitude

$$f_C(\theta) = \frac{Z_1Z_2e^2}{2\mu v^2 \sin^2(\theta/2)} \exp\left\{-i\eta \ln\left[\sin^2\left(\frac{\theta}{2}\right)\right] + i\pi + 2i\phi_0\right\}, \tag{13}$$

where $\phi_0 = \arg \Gamma(1 + i\eta/2)$. This is convenient for the numerical calculations since Eq. (6) is written with the separated contribution of the Coulomb-scattering amplitude. Then, the remaining integral (the second term on the RHS of Eq. (6)) converges rapidly for the scattering at forward angles. If we use Eqs. (10) and (11) the amplitude $F(\theta)$ cannot be separated as in Eq. (6) and the integral in b will converge very slowly.

A more important correction, due to the Coulomb deflection of the trajectory, amounts to calculating all elastic and inelastic integrals (to be discussed in Section 4) replacing the asymptotic impact parameter b by the distance of closest approach in Rutherford orbits, i.e.,

$$kb' = \eta + \sqrt{\eta^2 + k^2 b^2}\,. \tag{14}$$

As shown by Vitturi and Zardi [16] this correction leads to a considerable improvement of the eikonal amplitudes for the scattering of heavy systems.

For nucleus–nucleus collisions the spin–orbit interaction, $U_s(r)$, and the surface term of the imaginary potential (last term of Eq. (2)) are usually neglected. Whereas these terms are relevant for proton–nucleus scattering, they play no important role in nucleus–nucleus collisions. Thus, for nucleus–nucleus collisions, the scattering amplitude is given by

$$\frac{\mathrm{d}\sigma_{\mathrm{el}}}{\mathrm{d}\Omega} = |F(\theta)|^2, \tag{15}$$

where

$$F(\theta) = f_{\mathrm{C}}(\theta) + ik\int_0^\infty \mathrm{d}b\; bJ_0(qb)\,\exp[i\chi_{\mathrm{C}}(b)]\{1-\exp[i\chi_0(b)]\}. \tag{16}$$

Obviously, these equations can be obtained from Eqs. (5)–(7) by setting $\chi_s = 0$.

A common way to relate the nuclear optical potential to the ground-state densities is to use the "$t\rho\rho$" approximation. This approximation has been extensively discussed in the literature [12,13]. In its simplest version, neglecting the spin–orbit and surface terms, the optical potential for proton–nucleus collisions is given by

$$U_0(\boldsymbol{r}) = \langle t_{\mathrm{pn}}\rangle \rho_{\mathrm{n}}(\boldsymbol{r}) + \langle t_{\mathrm{pp}}\rangle \rho_{\mathrm{p}}(\boldsymbol{r}), \tag{17}$$

where ρ_{n} (ρ_{p}) are the neutron (proton) ground-state densities and $\langle t_{\mathrm{pi}}\rangle$ is the (isospin-averaged) transition matrix element for nucleon–nucleon scattering at forward directions,

$$t_{\mathrm{pi}}(\boldsymbol{q}=0) = -\frac{2\pi\hbar^2}{\mu} f_{\mathrm{pi}}(\boldsymbol{q}=0) = -\frac{\hbar v}{2}\,\sigma_{\mathrm{pi}}(\xi_{\mathrm{pi}} + i), \tag{18}$$

where σ_{pi} is the free proton–nucleon cross section and ξ_{pi} is the ratio between the imaginary and the real part of the proton–nucleon scattering amplitude. The basic assumption here is that the scattering is given solely in terms of the forward-proton–nucleon-scattering amplitude and the local one-body density [12].

For nucleus–nucleus collisions, we will use the same method which leads to an optical potential of the form

$$U_0(\boldsymbol{R}) = \int \langle t_{\mathrm{NN}}(\boldsymbol{q}=0)\rangle \rho_1(\boldsymbol{R}-\boldsymbol{r}')\,\rho_2(\boldsymbol{r}')\;\mathrm{d}^3r', \tag{19}$$

where $\boldsymbol{R}$ is the distance between the center-of-mass of the nuclei. We use the isospin average $\langle t_{\mathrm{NN}}\rangle = (t_{\mathrm{pp}} + t_{\mathrm{pn}})/2$.

Without much computational effort the formula (19) is improved to account for the scattering-angle dependence of the nucleon–nucleon amplitudes. A good parametrization [17] for the nucleon–nucleon scattering amplitude is given by $f_{NN}(q) = (k_{NN}/4\pi)\sigma_{NN}(i + \alpha_{NN})\exp(-\xi_{NN}q^2)$. The nuclear-scattering phase then becomes [14]

$$\chi_0(b) = \int\int \mathrm{d}\boldsymbol{r}\ \mathrm{d}\boldsymbol{r}'\ \rho_1(\boldsymbol{r})\gamma_{NN}(|\boldsymbol{b} - \boldsymbol{s} - \boldsymbol{s}'|)\rho_2(\boldsymbol{r}'), \tag{20}$$

where the profile function $\gamma_{NN}(b)$ is defined in terms of the two-dimensional Fourier transform of the elementary scattering amplitude,

$$\gamma_{NN} = \frac{1}{2\pi i k_{NN}} \int \exp(-i\boldsymbol{q}\cdot\boldsymbol{b}) f_{NN}(\boldsymbol{q})\ \mathrm{d}\boldsymbol{q}, \tag{21}$$

and $\boldsymbol{s}$, $\boldsymbol{s}'$ are the projections of the coordinate vectors $\boldsymbol{r}$, $\boldsymbol{r}'$ of the nuclear densities on the plane perpendicular to the z-axis. For spherically symmetric ground-state densities Eq. (20) simplifies to the expression

$$\chi_N(b) = \int_0^\infty \mathrm{d}q\ q\hat{\rho}_1(q) f_{NN}(q)\hat{\rho}_2(q) J_0(qb), \tag{22}$$

where $\rho_i(q)$ are the Fourier transforms of the ground-state densities.

In the following we will use Eq. (17) in order to calculate the proton–nucleus eikonal phase-shifts. For nucleus–nucleus collisions we will use the formula (22), since we assume the spherical symmetry for the ground-state distributions. We will now describe how we calculate the ground-state densities for exotic nuclei.

3. Ground-state densities

We calculate the density distributions of halo nuclei based on the Hartree–Fock (HF) approximation with Skyrme interaction. The Skyrme interaction is known to describe successfully the ground-state properties (the binding energies, the rms radii and the charge distributions) of many nuclei in a broad region of the mass table [18].

It was pointed out that the separation energy of loosely bound neutrons plays an important role in studying halo nuclei [19–21]. One needs an accuracy of about a few tens of keV to take into account the effect of the separation energy on the radii and the density distributions of halo nuclei, since they have extremely small separation energies as is shown in Table 1. On the other hand, the HF theory cannot provide the prediction for the separation energies within the accuracy of a few tens of keV [23]. It is known that higher-order effects beyond the mean-field approximation are necessary to describe more precisely the single-particle energies near the Fermi surface [24]. So far, several theoretical attempts [25] have been made in this direction, but the results do not satisfy the accuracy which is required for the study of halo nuclei. We take the following method [20,21,26] to improve the calculated separation energies rather than evaluating directly the higher-order effects; the last neutron configuration is treated differently from

Table 1
Single-neutron and two-neutron separation energies of neutron-rich nuclei. Data are taken from Ref. [22]

Nucleus	J^π	S_n (MeV)	S_{2n} (MeV)
^{6}He	0^+	1.86	0.97
^{8}He	0^+	2.58 ± 0.01	2.14 ± 0.05
^{9}Li	$\frac{3}{2}^-$	4.06	6.10
^{11}Li	$\frac{3}{2}^-$	0.73 ± 0.05	0.31 ± 0.05
^{11}Be	$\frac{1}{2}^+$	0.51	7.32
^{12}Be	0^+	3.17	3.67
^{14}Be	0^+	3.35 ± 0.11	1.34 ± 0.11

the other orbits in the HF potential in order to reproduce properly the neutron separation energy of the nucleus.

In the above procedure, the single-particle energy of the last orbit is adjusted to be the same as the empirical single-neutron separation energy in the case of the odd-N system, while the empirical two-neutron separation energy is adopted for the last neutron orbit in the even-N nucleus. Although it is not obvious how much the two-body correlation between the halo neutrons affects the single-particle wavefunction, this choice for the even-N nucleus was pointed out to be reasonable to study the Coulomb-dissociation cross sections ^{11}Li [9]. The soft dipole excitation in ^{11}Be [10] is also described well by this wavefunction.

The HF equation for the Skyrme interaction can be written as

$$\left(-\nabla \frac{\hbar^2}{2m^*(r)} \nabla + V(r) \right) \psi_\alpha(r) = \epsilon_\alpha \psi_\alpha(r), \tag{23}$$

Table 2
Calculated mass radii and observed interaction radii of halo nuclei. Radii of some halo orbits are also tabulated in the table. The core radii are obtained by the HF calculations, while the values for the halo configurations are calculated by using the renormalized potential (3). Data are taken from Refs. [2,3]

Nucleus	j_{last}	$\sqrt{\langle r^2 \rangle_{\text{cal}}}$ (fm)	$\sqrt{\langle r^2 \rangle_{\text{exp}}}$ (fm)
^{6}He		2.66	2.48 ± 0.03
^{8}He		2.59	2.49 ± 0.03
^{9}Li		2.45	2.41 ± 0.02
^{11}Li	$1p_{1/2}$	5.36	
		3.08	3.20 ± 0.03
^{11}Be	$2s_{1/2}$	6.29	
		3.01	2.86 ± 0.04
^{12}Be	$2s_{1/2}$	3.46	
		2.68	2.82 ± 0.04
^{14}Be	$2s_{1/2}$	5.28	
		3.16	3.33 ± 0.17

where $m^*(r)$ is the effective mass. The potential $V(r)$ has a central, a spin–orbit and a Coulomb term,

$$V(r) = V_{\text{central}} + V_{\text{spin-orbit}} + V_{\text{Coulomb}}. \tag{24}$$

This HF potential can be expressed analytically in terms of the parameters of the Skyrme interaction [18]. The central potential in Eq. (2) is multiplied by a constant normalization factor f only for the last neutron configuration:

$$V_{\text{central}}(r) = fV_{\text{HF}}(r), \quad \begin{cases} f \neq 1 & \text{for last neutron configuration,} \\ f = 1 & \text{otherwise.} \end{cases} \tag{25}$$

Numerical calculations are performed with the parameter set SGII [27] which gives satisfactory results for charge distributions of many nuclei, and also for the systematics of the nuclear radii in comparison with experimental data [28].

The empirical separation energies of light neutron-rich nuclei are tabulated in Table 1. Nuclei with negative values in Table 1 are unstable against neutron decay. We can see that the separation energies are extremely small in the cases of ^{6}He, ^{11}Li, ^{11}Be and ^{14}Be which are known as halo nuclei. Calculated radii are also tabulated in Table 2 together with empirical data.

4. Results for elastic scattering

We apply the formalism presented in Section 2 to the elastic scattering of stable nuclei in order to study the validity of the method. We will concentrate here on nuclei with spherical symmetry. The ground-state densities of stable nuclei used here are parametrized as gaussian (G) and modified Fermi (MF) densities, as shown in Table 3. The nucleon–nucleon cross sections used as input to construct the optical potentials in the "$t\rho\rho$" approximation are shown in Table 4. A linear interpolation is done to find the appropriate set of parameters at energies between those shown in the table. For energies lower than 94 MeV/nucleon we use $\xi_{\text{NN}} = 0.5$ fm^2. As one can deduce from Eq. (22) the q-dependence of f_{NN} with the parameters ξ_{NN}, as given in Table 4, is not important since the integrand in Eq. (22) is only relevant for $q < 1/b \ll 1/\sqrt{\xi_{NN}}$.

Table 3
Parameters of the ground-state densities of stable nuclei which are given by either gaussian (G) or modified fermi (MF) distributions. Data are taken from Ref. [29]

Nucleus	Model	R	a	c
α	G	1.37	–	–
^{11}C	MF	2.34	0.5224	−0.149
^{12}C	MF	2.34	0.5224	−0.149
^{16}O	MF	2.61	0.513	−0.051
^{17}O	MF	2.61	0.513	−0.051
^{208}Pb	MF	6.62	0.549	0

Table 4
Parameters [17] for the nucleon–nucleon amplitude, $f_{NN}(q)=(k_{NN}/4\pi)\sigma_{NN}(i+\alpha_{NN})\exp(-\xi_{NN}q^2)$

E (MeV/nucleon)	σ_{NN} (fm^2)	α_{NN}	ξ_{NN} (fm^2)
30	19.6	0.87	
38	14.6	0.89	
40	13.5	0.9	
49	10.4	0.94	
85	6.1	1	
94	5.5	1.07	0.51
120	4.5	0.7	0.58
200	3.2	0.6	0.62
342.5	2.84	0.26	0.31
425	3.2	0.36	0.24
550	3.62	0.04	0.062
650	4.0	−0.095	0.08
800	4.26	−0.075	0.105
1000	4.32	−0.275	0.105
2200	4.33	−0.33	0.13

In Fig. 1 we show the experimental data from Ref. [30] for the elastic scattering of $^{17}O + ^{208}Pb$ at 84 MeV/nucleon. The curve is calculated using the nuclear phase-shift constructed as in Eq. (22) and the scattering amplitude as in Eq. (16). We observe that the agreement with the data is extremely good. The rainbow scattering at $\theta \sim 2.5°$ is also very well reproduced. However, one should be cautious with such an example since in this case the scattering amplitude is dominated by a sharp transition from no absorption to strong absorption as the scattering angle increases. Basically, the optical potential has

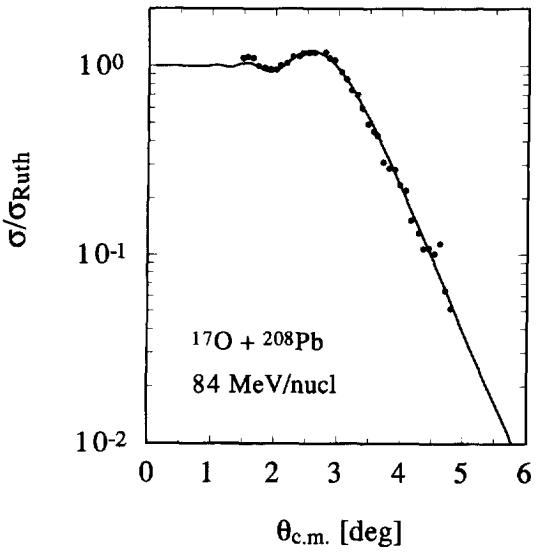

Fig. 1. Elastic-scattering cross section of $^{17}O+^{208}Pb$ at 84 MeV/nucleon. The data points are from Ref. [30]. The solid curve is a calculation with the "$t\rho\rho$" approximation.

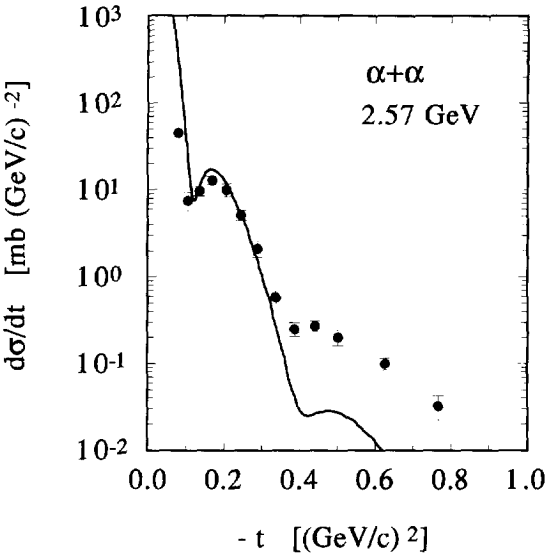

Fig. 2. Elastic-scattering cross section of $\alpha + \alpha$ at $E_{lab} = 2.57$ GeV as a function of the invariant momentum transfer $t = -(p_1 + p_2)^2$. The data points are from Ref. [31]. The solid curve is a calculation with the "$t\rho\rho$" approximation.

to have the feature of a large absorption at small distances and a small diffuseness. This behavior arises naturally within the framework of the "$t\rho\rho$" approximation for heavy systems.

Light systems are more "transparent" and the collision at small distances (large scattering angle) are more sensitive to the details of the optical potential. To show this we plot in Fig. 2 the elastic scattering of $\alpha + \alpha$ at $E_{lab} = 2.57$ GeV as a function of the invariant momentum transfer $t = -(p_1 + p_2)^2$. The data are from Ref. [31]. The calculated curve agrees reasonably well with the data at forward angles (small t) but deviates appreciably from it at larger angles. The forward scattering is dominated by peripheral collisions for which multiple scattering is not relevant. Thus, we expect that the "$t\rho\rho$" approximation works well at forward angles. On the other hand, it has been shown that multiple collisions are very important for large scattering angles [32], so that the "$t\rho\rho$" approximation fails to explain the data.

We plot in Fig. 3 the elastic scattering of $^{12}C + ^{12}C$ at $E_{lab} = 85$ MeV/nucleon to study the model further. The data are from Ref. [33]. The solid curve is obtained by using the eikonal approximation (Eqs. (16) and (22)) with a set of Woods–Saxon (WS) potentials which was constructed to give the smaller χ-square fit to the data with a DWBA calculation using the code PTOLEMY [34]. This Woods–Saxon potential reproduces the data perfectly [33]. The parameters obtained by this fit are

$$\begin{aligned} V_0 &= -120 \text{ MeV}, \quad R_v = 1.72 \text{ fm}, \quad \text{and} \quad a_v = 0.83 \text{ fm} \\ W_0 &= -46.8 \text{ MeV}, \quad R_w = 2.2 \text{ fm}, \quad \text{and} \quad a_w = 0.86 \text{ fm}. \end{aligned} \tag{26}$$

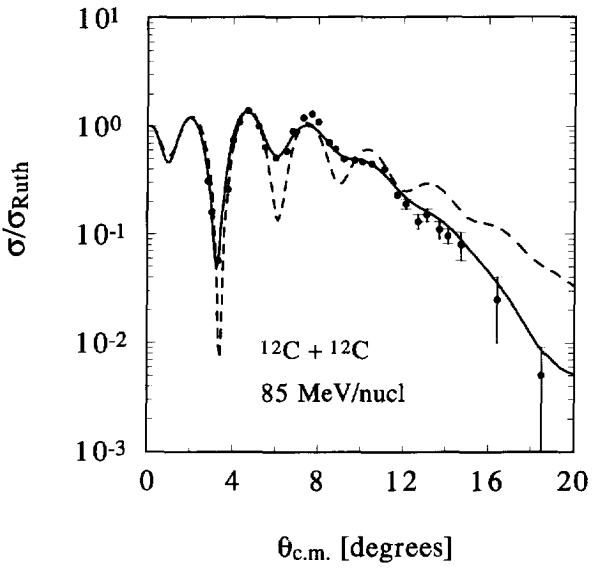

Fig. 3. Elastic-scattering cross section of $^{12}C+^{12}C$ at $E_{lab}=85$ MeV/nucleon. The solid curve uses the eikonal approximation and the WS optical-potential parameters given by Eq. (26). The dashed curve uses the "$t\rho\rho$" approximation. The data are taken from Ref. [33].

The dashed curve is obtained with the "$t\rho\rho$" approximation which shows again the mismatch with the data at large scattering angles. We see that the "$t\rho\rho$" approximation gives a reasonable description of the elastic scattering only at forward angles. It is known that large scattering angles are affected by corrections due to real, and virtual, (polarization) nuclear excitation [35]. This means that a simple and unambiguous relationship between the elastic-scattering data and the nuclear ground-state densities does not exist at large scattering angles. We conclude that the disagreement between the experimental data and the method used here, for light systems and large scattering angles, is not a deficiency of the eikonal approximation, but of the construction of the optical potential (i.e. of the assumption of the validity of the "$t\rho\rho$" approximation).

The corrections due to multiple collisions using the Glauber multiple-scattering series is rather cumbersome [32] and a direct connection between the ground-state densities of the nuclei and the scattering data is lost among a large variety of approximations. We feel that, due to its simplicity, the "$t\rho\rho$" approximation is very appealing within its limitations. We therefore will use this approximation since the complications arising from a treatment of multiple scattering, and of other effects, undermines our effort to extract information about the ground-state densities of the nuclei from the elastic scattering. We will focus in the following study mainly on the forward-scattering region because of the limited validity of the model.

Fig. 4a shows the elastic scattering of a proton off ^{9}Li at $E_{lab}=60$ MeV/nucleon. The data are from Ref. [4]. The solid curve is obtained by using Eqs. (5)–(7) with the parameters shown in Table II of Ref. [4] which was obtained by a χ-square fitting to the

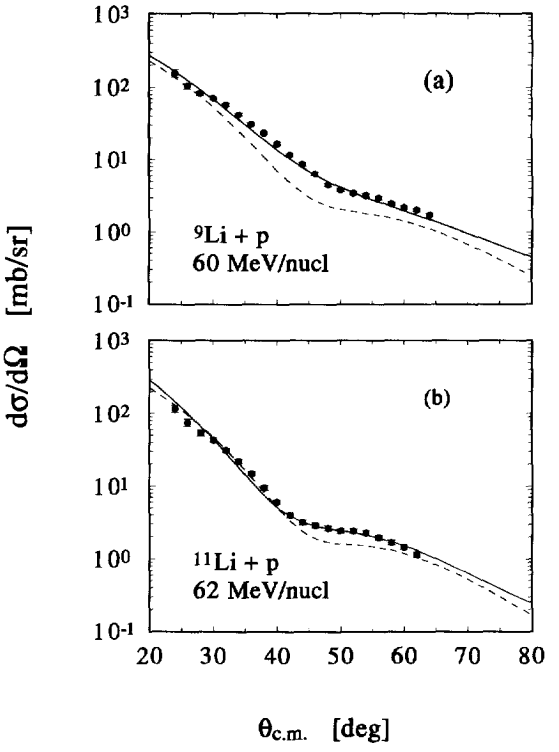

Fig. 4. (a) p + ^{9}Li elastic scattering at $E_p = 60$ MeV. The data are from Ref. [4]. (b) p + ^{11}Li elastic scattering at $E_p = 62$ MeV. The data are from Ref. [4]. The solid curves are obtained by using the optical potential as in Eqs. (1)–(3) with the same set of parameters as used in Ref. [4]. The dashed curves use "$t\rho\rho$" potentials constructed as in Eqs. (17)–(19).

data with a DWBA calculation. The dashed curve is obtained by using the optical potential constructed as in Eqs. (17)–(19) together with the Hartree–Fock ^{9}Li ground-state density. In this case the surface and spin–orbit interactions are absent. The dashed curve clearly misses the experimental data. The absorption is greater than expected by the "$t\rho\rho$" method so that this difference cannot be ascribed only to the absence of the spin–orbit interaction. Quite a different scenario is presented in Fig. 4b where we plot the p + ^{11}Li scattering data at 62 MeV/nucleon from Ref. [4]. The solid curve is calculated with the optical-potential parameters of Table II (set B) of Ref. [4] for Eqs. (1)–(3), which were chosen so as to fit the experimental data. The dashed curve is obtained by using Eqs. (17)–(19) and the ^{11}Li Hartree–Fock ground-state density, calculated as explained in Section 2. The agreement with the data is quite good at forward angles, in contrast to the previous case.

One might think that the good quantitative description obtained in Fig. 4b is accidental, in view of the previous discussions. In order to clarify further the validity of the model, we show in Fig. 5 the elastic-scattering data of p + ^{8}He at 72 MeV/nucleon together with a calculation using the optical potential constructed as in Eqs. (17)–(19)

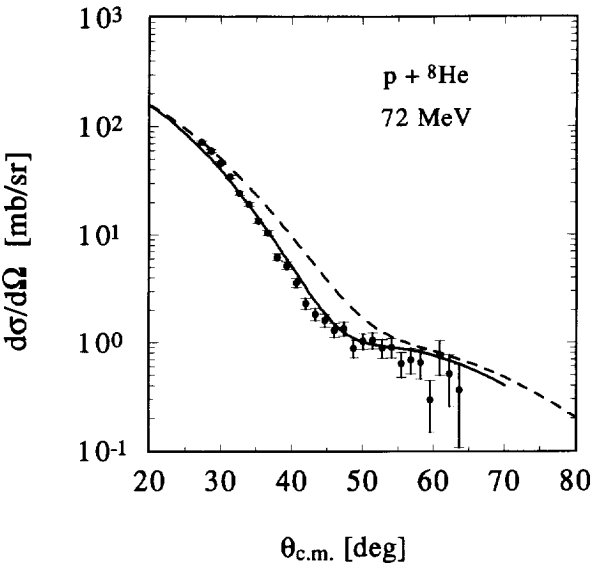

Fig. 5. Elastic-scattering cross section for p+^{8}He at 72 MeV/nucleon. The solid curve is a calculation using Eqs. (17)–(19), while the dashed curve is for the system p+^{6}He at the same bombarding energy. The data are from Ref. [5].

by the solid curve. The ground-state density of ^{8}He was calculated as explained in Section 3. Although the data uncertainties at $\theta > 40°$ do not allow for a test of the theory, the agreement with the data is almost perfect at forward angles. Such an agreement is very encouraging since the simple "$t\rho\rho$" approach is of very useful predictive power and it can be used to plan future experiments on radioactive beams scattering off protons. Also shown in Fig. 5, the dashed curve is the scattering cross section obtained by using the ^{6}He ground-state density. Two important features are seen. Firstly, the strength of the strong absorption in the p + ^{8}He system is appreciably larger than in the p + ^{6}He system. Secondly, the diffraction minimum is at a larger angle for ^{6}He targets than for the ^{8}He ones, revealing a larger absorption radius of ^{8}He.

The inclusion of the surface and spin–orbit terms of Eq. (1) in a microscopic Glauber approach, as in Eq. (17), to elastic scattering is rather complicated (see discussion in Ref. [12]). The absence of these terms in our approach may be considered as one of the main reasons for the discrepancies between the experimental data and the calculations. This problem should not occur for nucleus–nucleus collisions, since the folding of densities "smear out" the surface and spin–orbit terms of the nucleon–nucleus optical potential.

Data on the elastic scattering of halo nuclei have been taken during the last few years. Due to the poor energy resolution, the data are contaminated with inelastic scattering. In Figs. 6, 7 and 8 we plot the data on quasi-elastic scattering of ^{11}Li + ^{12}C at $E_{\rm lab} = 637$ MeV, of ^{12}Be + ^{12}C at $E_{\rm lab} = 679$ MeV, and of ^{14}Be + ^{12}C at $E_{\rm lab} = 796$ MeV, respectively. The dashed curves are calculated by using the prescription given by Eqs.

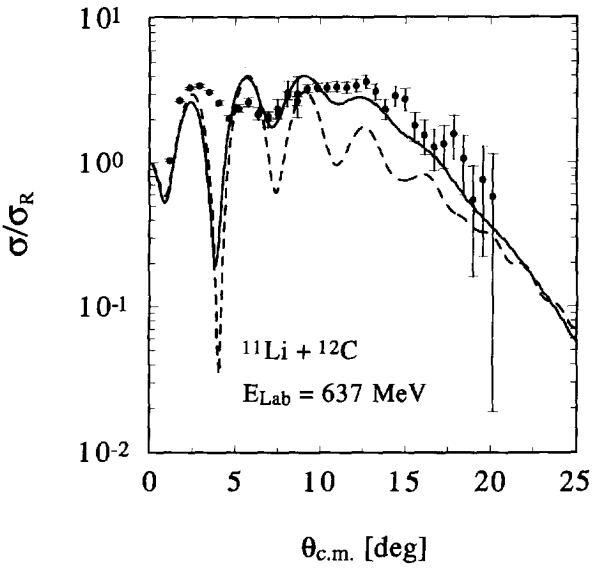

Fig. 6. Quasi-elastic scattering of $^{11}Li + ^{12}C$ at $E_{lab} = 637$ MeV. The data are from Ref. [6]. The inelastic contribution to the cross section was added to the elastic cross section (solid figure). The pure elastic cross section is given by the dashed curve. The deformation parameters $\beta_2 = 0.59$ and $\beta_3 = 0.40$ for the 2^+ and 3^- states in ^{12}C were used.

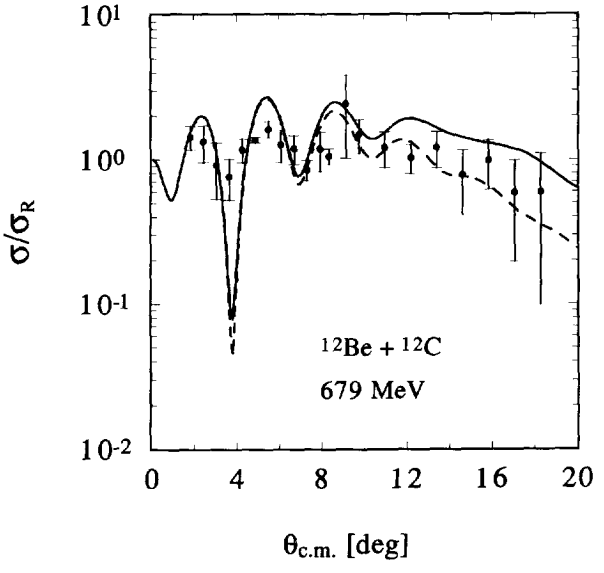

Fig. 7. Quasi-elastic scattering of $^{12}Be + ^{12}C$ at $E_{lab} = 679$ MeV. The data are from Ref. [7]. The inelastic contribution to the cross section was added to the elastic cross section (solid figure). The pure elastic cross section is given by the dashed curve. The deformation parameters $\beta_2 = 0.59$ and $\beta_3 = 0.40$ for the 2^+ and 3^- states in ^{12}C were used.

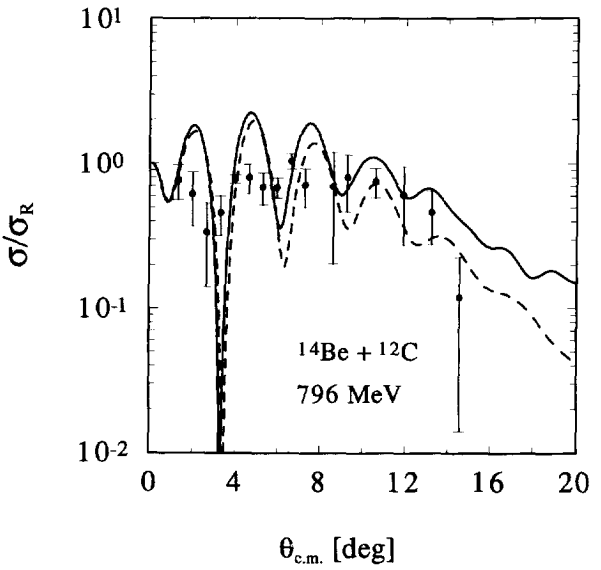

Fig. 8. Quasi-elastic scattering of $^{14}Be + ^{12}C$ at $E_{lab} = 796$ MeV. The data are from Ref. [7]. The inelastic contribution to the cross section was added to the elastic cross section (solid figure). The pure elastic cross section is given by the dashed curve. The deformation parameters $\beta_2 = 0.59$ and $\beta_3 = 0.40$ for the 2^+ and 3^- states in ^{12}C were used.

(15), (16), (22) and the Hartree–Fock densities calculated as explained in Section 2. The data are from Refs. [6,7]. While the agreement is quite reasonable for the $^{12}Be + ^{12}C$ and $^{14}Be + ^{12}C$ data, it does not work so well for the $^{11}Li + ^{12}C$ data. The solid curves are calculated by including the inelastic excitation of the 2^+ and the 3^- states in ^{12}C which cannot be separated from the experimental data. In the next section we describe how to calculate the inelastic-scattering-excitation cross sections. We use the deformed-potential model for the excitation of ^{12}C, with deformation parameters $\beta_2 = 0.59$ and $\beta_3 = 0.40$ for the 2^+ and the 3^- states, respectively. These are the same values as used in Refs. [6,7]. We observe that, with the inclusion of inelastic scattering, the theoretical results for the $^{11}Li + ^{12}C$ collision are remarkably good, but the ones for $^{12}Be + ^{12}C$ and for $^{14}Be + ^{12}C$ are not, yielding too large cross sections at large angles. One possible reason for such a discrepancy is the absence of dynamical polarization in our approach. The virtual excitations during the collision time are shown to affect the elastic scattering of the halo neutron appreciably and have been studied by several authors [36]. An inclusion of such effects is beyond our model of using a simplified approach to study the ground-state properties of the halo nuclei. Another possibility is that the folding prescription to determine the optical potential yields larger cross sections than the experimental ones, as we observed in Fig. 3.

We conclude that the simple "$t\rho\rho$" folding procedure is a useful method to describe quantitatively the elastic-scattering data of radioactive nuclei in most cases. We should also notice that the inelastic scattering makes it difficult to obtain good agreement with

the data, especially at larger angles. However, a test of the ground-state densities of such nuclei is possible by comparing the data with the theoretical calculations at forward angles. At large angles, especially with the presence of inelastic scattering, the results are, however, sometimes misleading. More detailed microscopic calculations would be necessary to obtain better agreement. In the opposite extreme, one may resort to the use of optical potential parameters to fit the data. In both cases, a link of the results to microscopic features of the nuclei is very difficult to achieve.

5. Inelastic scattering

5.1. Nuclear excitation

We can use the distorted-wave approximation (DWBA) for the inelastic amplitude, assuming that a residual interaction U between the projectile and the target exists and is weak. The cross section for the excitation of a vibrational mode $(\lambda\mu)$ with energy $\hbar\omega_\lambda$ is given by

$$\frac{\mathrm{d}\sigma_{\lambda\mu}}{\mathrm{d}\Omega} = \frac{k_\lambda}{k_0}|f_{\lambda\mu}(\theta)|^2 = \left(\frac{M}{2\pi\hbar^2}\right)^2 \frac{k_\lambda}{k_0}\left|\left\langle \Psi_{\lambda\mu}\phi^{(-)}_{k_\lambda}\middle|U\middle|\Psi_0\phi^{(+)}_{k_0}\right\rangle\right|^2, \tag{27}$$

where k_λ is defined as

$$E_{k_\lambda} = \frac{\hbar^2 k_\lambda^2}{2M} = \frac{\hbar^2 k_0^2}{2M} - \hbar\omega_\lambda. \tag{28}$$

In Eq. (28), M is equal to the reduced mass of the system and k_0 is equal to their relative momentum. The wavefunctions ϕ and Ψ describe the relative motion and the internal states, respectively.

In the particle-vibration-coupling model the transition matrix elements are given by

$$M_{\lambda\mu}(r) \equiv \langle \Psi_{\lambda\mu}|U|\Psi_0\rangle = \frac{\delta_\lambda}{\sqrt{2\lambda+1}} Y_{\lambda\mu}(\hat{r})U_\lambda(r), \tag{29}$$

where $\delta_\lambda = \beta_\lambda R$ is the vibrational amplitude, or *deformation length*, R is the nuclear radius and $U_\lambda(r)$ is the transition potential. We will consider only low multipolarities, $l \leqslant 2$ in the following.

The deformation length δ_λ can be directly related to the reduced matrix elements for electromagnetic transitions. Using well-known sum-rules for these matrix elements one finds a relation between the deformation length, the nuclear sizes and the excitation energies. For isoscalar excitations one obtains [37]

$$\delta_0^2 = 2\pi\frac{\hbar^2}{m_N}\frac{\langle r^2\rangle}{AE_x}, \quad \delta^2_{\lambda\geqslant 2} = \frac{2\pi}{3}\frac{\hbar^2}{m_N}\lambda(2\lambda+1)\frac{1}{AE_x}, \tag{30}$$

where A is the atomic number, $\langle r^2\rangle$ is the rms radius of the nucleus and E_x is the excitation energy.

The transition potentials for isoscalar excitations are

$$U_0(r) = 3U_{\rm opt}(r) + r\frac{{\rm d}U_{\rm opt}(r)}{{\rm d}r} \tag{31}$$

for monopole and

$$U_2(r) = \frac{{\rm d}U_{\rm opt}(r)}{{\rm d}r} \tag{32}$$

for quadrupole modes.

For dipole isovector excitations, the deformation length is given by

$$\delta_1 = \pi\frac{\hbar^2}{2m_{\rm N}}\frac{A}{NZ}\frac{1}{E_{\rm x}}, \tag{33}$$

where Z (N) is the charge (neutron) number. The transition potential in this case is [37]

$$U_1(r) = \gamma\frac{N-Z}{A}\left(\frac{{\rm d}U_{\rm opt}}{{\rm d}r} + \tfrac{1}{3}R_0\frac{{\rm d}^2U_{\rm opt}}{{\rm d}r^2}\right), \tag{34}$$

where the factor γ depends on the difference between the proton- and the neutron-matter radii as

$$\gamma\frac{2(N-Z)}{3A} = \frac{R_{\rm n}-R_{\rm p}}{\frac{1}{2}(R_{\rm n}+R_{\rm p})} = \frac{\Delta R_{\rm np}}{R_0}. \tag{35}$$

Thus, the strength of isovector excitations increases with the difference between the neutron- and the proton-matter radii. This difference is accentuated for neutron-rich nuclei so that the isovector dipole excitations should be a good test for the quantity $\Delta R_{\rm np}$ which becomes very large for neutron-rich unstable nuclei. One can generalize this equation to higher isovector multipole excitations $\lambda \geqslant 2$ by the substitution

$$\frac{N-Z}{A} \to Q_\lambda^{(\rm n)} + Q_\lambda^{(\rm p)} = Z\left(-\frac{1}{A}\right)^\lambda + \left[\left(1-\frac{1}{A}\right)^\lambda + (-1)^\lambda\frac{Z-1}{A^\lambda}\right], \tag{36}$$

where $Q_\lambda^{(\rm n,p)}$ are the effective charges (in units of e) of the neutron and the proton, respectively.

A useful approximation, valid for $\hbar\omega_\lambda \ll E_{k_\lambda}$, is

$$k_\lambda \simeq k_0\left(1-\frac{M\omega_\lambda}{\hbar k_0^2}\right) = k_0 + \frac{\omega_\lambda}{v}. \tag{37}$$

Further, by using the definition (27) and the eikonal approximation

$$\phi_{k_\lambda}^{(-)*}\phi_{k_0}^{(+)} \simeq \exp\left[iq\cdot r + i\chi(b)\right], \tag{38}$$

we get

$$f_{\lambda\mu}(\theta) = \frac{M}{2\pi\hbar^2}\frac{1}{\sqrt{\lambda+1}}\delta_\lambda i^\mu\sqrt{\pi(2\lambda+1)}\sqrt{\frac{(\lambda-\mu)!}{(\lambda+\mu)!}}\int_0^\infty {\rm d}b\, bJ_\mu(q_t b)$$
$$\times {\rm e}^{i\chi(b)}\int_{-\infty}^{\infty}{\rm d}z\, P_{\lambda\mu}\left(\frac{z}{\sqrt{b^2+z^2}}\right)U_\lambda(b,z)\exp\left(\frac{i\omega_\lambda z}{v}\right), \tag{39}$$

where J_μ and $P_{\lambda\mu}$ are the Bessel function and the Legendre polynomials, respectively, and $q_t = 2\sqrt{k_0 k_\lambda}\,\sin(\theta/2)$.

As seen in Eq. (39), one needs to calculate two simple integrals to compute the inelastic scattering at intermediate energies with the deformed-potential model. The scattering amplitudes will depend on the optical-potential parameters and on the deformation length δ_λ. The deformed-potential model is based on the assumption of a transition density peaked at the surface. Although this assumption is reasonable for the excitation of heavy nuclei (e.g., ^{40}Ca, ^{208}Pb), it is rather crude for light nuclei, especially when the transition density extends radially beyond the nuclear size. This is the case for the soft multipole excitations, for which the transition densities have very long tails.

A more convenient way to describe the inelastic scattering of neutron-rich nuclei is to use the folding approximation. The assumption of a transition density peaked at the surface of the nucleus is not necessary. In this model the matrix element on the RHS of Eq. (27) is

$$T_{\lambda\mu} = \int \mathrm{d}^3R \int \mathrm{d}^3r\; \phi^{(-)*}_{\boldsymbol{k}_\lambda}(\boldsymbol{R}) U_{\mathrm{int}}(|\boldsymbol{R}-\boldsymbol{r}|)\,\delta\rho_{\lambda\mu}(\boldsymbol{r})\;\phi^{(+)}_{\boldsymbol{k}_0}(\boldsymbol{R}), \tag{40}$$

where $\delta\rho_{\lambda\mu} = \Psi^*_{\lambda\mu}\Psi_0$ is the transition density. $U_{\mathrm{int}}(|\boldsymbol{R}-\boldsymbol{r}|)$ is the potential between each nucleon of the target and the projectile nucleus. Thus, the transition from the ground state to the excited state is directly calculated from the target-nucleon–projectile interaction.

For light targets, a gaussian parametrization of the target-nucleon–projectile potential is adequate and yields simple formulas. This can be shown by means of the expansion

$$\begin{aligned} U_{\mathrm{int}}(|\boldsymbol{R}-\boldsymbol{r}|) &= (v_0 + iw_0)\,\exp\left(-\frac{(\boldsymbol{R}-\boldsymbol{r})^2}{a^2}\right) \\ &= 4\pi(v_0+iw_0)\,\exp\left(-\frac{R^2+r^2}{a^2}\right) \\ &\quad\times\sum_{\lambda\mu} i^\lambda j_\lambda\left(2i\frac{rR}{a^2}\right) Y_{\lambda\mu}(\hat{\boldsymbol{R}})\,Y^*_{\lambda\mu}(\hat{\boldsymbol{r}}), \end{aligned} \tag{41}$$

where the $j_\lambda(ix)$ are the spherical Bessel functions calculated for imaginary arguments.

Using this result in Eq. (27) and the definition $\delta\rho(\boldsymbol{r}) = \delta\rho_\lambda(r)Y_{\lambda\mu}(\hat{\boldsymbol{r}})$, we get (using $\boldsymbol{R} = (\boldsymbol{b}, Z)$)

$$\begin{aligned} T_{\lambda\mu} &= 4\pi^{3/2}(v_0+iw_0)\sum_{\lambda\mu} i^{\lambda\mu}\sqrt{\frac{(2\lambda+1)(\lambda-\mu)!}{(\lambda+\mu)!}} \\ &\quad\times\int_0^\infty \mathrm{d}b\; bJ_\mu(q_t b)\;\mathrm{e}^{i\chi(b)}\mathscr{O}_{\lambda\mu}(b), \end{aligned} \tag{42}$$

where

$$\mathscr{O}_{\lambda\mu}(b) = \int_0^\infty \mathrm{d}r\; r^2\delta\rho_{\lambda\mu}(r)\;F_{\lambda\mu}(r,b), \tag{43}$$

with

$$F_{\lambda\mu}(r,\, b) = \int_{-\infty}^{\infty} \mathrm{d}Z \, \exp\left(-\frac{R^2+r^2}{a^2}\right) j_\lambda\left(\frac{2irR}{a^2}\right) P_{\lambda\mu}\left(\frac{Z}{R}\right) \exp\left(i\frac{\omega_\lambda Z}{v}\right). \tag{44}$$

A link between the deformed-potential model and the folding model is obtained by using the approximation

$$\delta\rho_\lambda = -\begin{cases} \dfrac{\delta_\lambda}{\sqrt{2\lambda+1}}\dfrac{\mathrm{d}\rho_0}{\mathrm{d}r}, & \text{for } \lambda \geqslant 1, \\ \delta_0\left(3\rho_0 + r\dfrac{\mathrm{d}\rho_0}{\mathrm{d}r}\right), & \text{for } \lambda = 0. \end{cases} \tag{45}$$

As in the deformed-potential model, the scattering amplitude is determined by the optical-potential parameters and the deformation length δ_λ.

Another common approximation for $\delta\rho_\lambda$ is provided by the Tassie model [38] which gives

$$\delta\rho_\lambda(r) = -\frac{\delta_\lambda}{\sqrt{2\lambda+1}}\left(\frac{r}{R_0}\right)^{\lambda-1}\frac{\mathrm{d}\rho_0}{\mathrm{d}r}, \quad \text{for } \lambda \geqslant 1. \tag{46}$$

For $\lambda = 0$, one uses Eq. (45). In general, both models yield analogous transition densities for heavy nuclei and low collective states.

These approximations assume that the transition density is peaked at the nuclear surface. As we discussed in Ref. [11], this is a bad approximation for neutron-rich nuclei. It is more convenient to directly use the transition density calculated from microscopic models and inserted into Eqs. (42) and (43) to obtain the scattering amplitude.

5.2. Coulomb excitation

The subject of Coulomb excitation for heavy-ion collisions at intermediate energies has been discussed in Ref. [39], including retardation and strong-absorption effects. The Coulomb-excitation amplitude for a given multipolarity Eλ is given by

$$f_{\mathrm{E1},\mu}(E_\mathrm{x},\, \theta) = i\frac{\sqrt{8\pi}}{3}\frac{Z_\mathrm{T} e M_{aA}}{\hbar^2}\frac{E_\mathrm{x}}{\hbar v_a}\left[B(\mathrm{E1},\, E_\mathrm{x})\right]^{1/2} \times \begin{cases} A_{\pm 1}(E_\mathrm{x},\, \theta), & \text{for } \mu = \pm 1, \\ A_0(E_\mathrm{x},\, \theta), & \text{for } \mu = 0 \end{cases} \tag{47}$$

for E1 excitations and

$$f_{\mathrm{E2},\mu}(E_\mathrm{x},\, \theta) = -\frac{2}{5}\frac{\sqrt{\pi}}{6}\frac{Z_\mathrm{T} e M_{aA}}{\hbar^2}\left(\frac{E_\mathrm{x}}{\hbar v_a}\right)^2\left[B(\mathrm{E2},\, E_\mathrm{x})\right]^{1/2} \times \begin{cases} A_{\pm 2}(E_\mathrm{x},\, \theta)/\gamma, & \text{for } \mu = \pm 2, \\ -(2 - v^2/c^2)A_{\pm 1}(E_\mathrm{x},\, \theta), & \text{for } \mu = \pm 1, \\ A_0(E_\mathrm{x},\, \theta), & \text{for } \mu = 0 \end{cases} \tag{48}$$

for E2 excitations.

In the above equations $\gamma = (1 - v_a^2/c^2)^{-1/2}$, and μ is the azimuthal component of the transferred angular momentum. The functions Λ_μ are given by

$$\Lambda_\mu(E_x, \theta) = \int_0^\infty db\, bJ_\mu(qb) K_\mu\left(\frac{E_x b}{\gamma \hbar v_a}\right) \exp[i\chi(b)], \tag{49}$$

where $q = 2k \sin(\theta/2)$, k is the c.m. momentum of $a + A$, and the J_μ (K_μ) are Bessel (modified) functions of order μ. $\chi(b) = \chi_N(b) + \chi_C(b)$ is obtained from Eqs. (8) and (9).

Assuming that an isolated state is excited, and that it fully exhausts the sum-rules, one gets ($B(E\lambda) \equiv B(E\lambda, E_x)$)

$$B(E1) = \frac{9}{4\pi} \frac{\hbar^2}{2m_N} \frac{NZ}{AE_x} e^2 \tag{50}$$

and

$$B(E2) = \frac{\hbar^2}{m_N} \frac{15R^2}{4\pi E_x} e^2 \begin{cases} Z^2/A, & \text{for isoscalar excitations,} \\ NZ/A, & \text{for isovector excitations.} \end{cases} \tag{51}$$

The electromagnetic-transition operators have a smooth dependence on the spatial coordinates ($\mathcal{O}(E1) \sim r$ and $\mathcal{O}(E2) \sim r^2$). Thus, the electromagnetic excitation has a very weak dependence on the spatial form of the transition density and it does not seem to be a direct probe of the halo properties. However, the reduced matrix elements for halo nuclei are expected to be enhanced due to unique properties of the halo wavefunctions. For example, if the binding of the valence neutrons is very weak, as in the case of ^{11}Li, one expects a huge enhancement of the $B(E1)$ strength at low energies (soft E1 modes). This can be thought of as being due to the threshold effect of extended halo neutrons with respect to the core, which leads to large $B(E1)$ values.

6. Results for inelastic scattering

We first apply the formulation of the previous section to the inelastic scattering of stable nuclei. In Fig. 9 we plot the inelastic scattering of 84 MeV/nucleon ^{17}O projectiles on lead. The excitation of the isoscalar giant quadrupole resonance in lead ($E_x = 10.9$ MeV) is considered. The data points are from Ref. [30]. The curves are calculated by using the deformed-potential model. The optical potential was calculated by using the folding procedure described in Section 2. The deformation parameter $\beta_2 = 0.63$ was used. This corresponds to 100% of exhaustion of the sum-rule. The dashed curve is the contribution of the Coulomb excitation with $B(E2) = 0.73\ e^2b^2$, also corresponding to 100% of the sum rule (51). The dotted curve is the nuclear contribution only and the solid curve includes both contributions and their interference. We see that the scattering data are very reasonably described by this approach. The excitation of the isovector electric-dipole giant resonance in the same system is

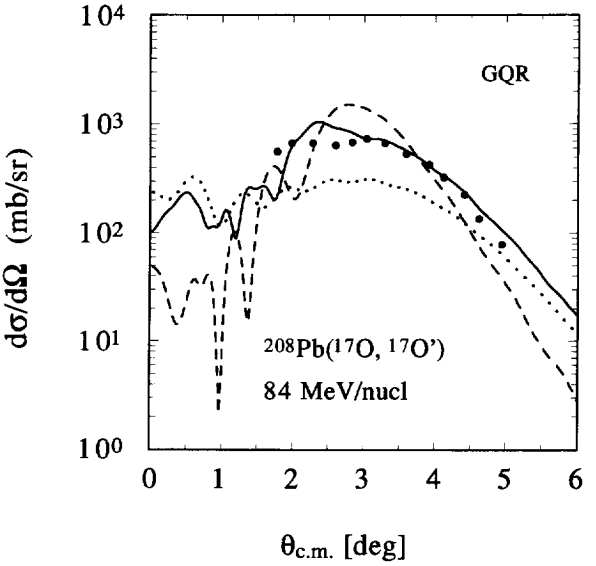

Fig. 9. Excitation cross section of the giant quadrupole resonance in ^{208}Pb in the reaction $^{17}O+^{208}Pb$ at 84 MeV/nucleon. The data are from Ref. [30]. The optical potential was calculated by the "$t\rho\rho$" approximation. The deformed-potential model is used to calculate the nuclear-excitation cross section which is drawn by a dotted curve. The dashed curve is the Coulomb-excitation cross section. The total cross section due to Coulomb and to nuclear excitations is shown by the solid curve.

dominated by the Coulomb interaction and is also well described by eqs. (47), (48), as shown in Ref. [39].

In general, both the deformed-potential model and the folding model give very good agreement with the experimental data for the inelastic scattering of stable nuclei. This has been studied extensively, e.g., in Ref. [37]. Also, in Ref. [11] it was shown that a good agreement with the experimental data for the excitation of giant monopole and giant quadrupole resonances in lead by 172 MeV α's is obtained with the use of Eqs. (42)–(44), based on the eikonal approximation. The details of the oscillatory pattern of the angular distributions are easily understood in terms of the Bessel function $J_\mu(q_t b)$ in Eq. (42).

An interesting application of this formalism is to the excitation of a Roper resonance ($E_x = 500$ MeV) in the $\alpha + p$ reaction with $E_\alpha = 4.2$ GeV. This is shown in Fig. 10, together with the data points taken from Ref. [40]. The data show a very steep angular dependence, characteristic of a monopole transition. As shown by the authors of Ref. [40], the angular distribution can be well described by assuming that the Roper resonance is a monopole excitation, exhausting a large fraction of the monopole sum-rule, Eq. (30). The solid curve in the figure is calculated by using a folding potential derived according to Eq. (17) and the transition amplitude calculated within the deformed-potential model, Eq. (39), and using δ_0 calculated as in Eq. (30), with $\langle r_p^2 \rangle = 3R^2/5 = 0.69$ fm^2 (and $A = 1$). The agreement with the data is remarkably good and the value of $\langle r_p^2 \rangle$ is in reasonable agreement with the predictions for the

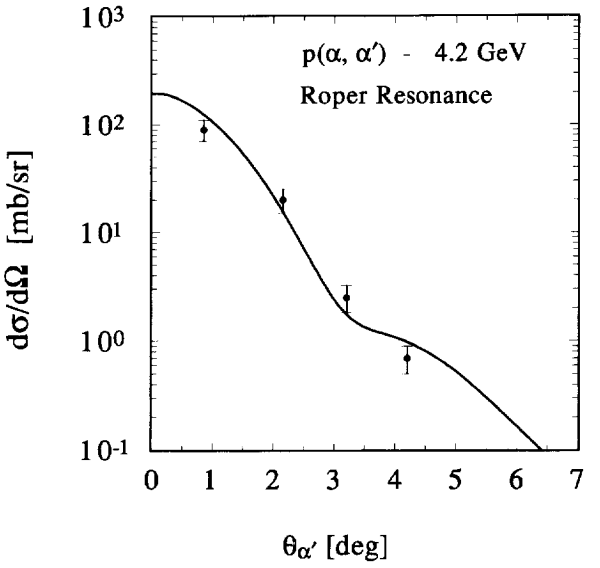

Fig. 10. Angular dependence of the inelastic cross section for the excitation of the Roper resonance in a proton with the reaction $\alpha + p$ at $E_\alpha = 4.2$ GeV. The data points are from Ref. [40]. The solid curve is calculated by using the deformed-potential model.

electromagnetic radius of the nucleon in models which include sea-quark polarization effects [41].

To our knowledge, up to the present date very few experimental data exist on the inelastic scattering of exotic nuclei. Using the formalism in Eqs. (40)–(44), predictions for the inelastic excitation of soft monopole and quadrupole modes in the ^{11}Li incident on carbon targets have been done [11]. It was shown that the particular oscillatory pattern of the excitation cross sections could be an important tool to identify different excited states in these nuclei. This is a well-known method in reactions with stable nuclei, which allows one to distinguish, e.g., monopole from quadrupole excitations. The extension of the halo in loosely bound nuclei would also affect appreciably the drop in magnitude of these cross sections with increasing scattering angle [11].

In Fig. 11 we plot the excitation cross section for the 2^+ state ($E_x = 3.57$ MeV) in ^{8}He by 72 MeV protons. The data are from Ref. [5]. We used the folding model for the calculation of the optical potential. The inelastic cross section was calculated with the deformed-potential model and a deformation parameter $\beta_2 = 0.32$. As seen, the agreement with the data is quite good.

Finally we discuss the Coulomb excitation of exotic nuclei. As an example we consider the Coulomb excitation of ^{11}Be projectiles with 45 MeV/nucleon incident on lead targets. We consider the electric-dipole excitation of the $\frac{1}{2}^+$ ground state to the $\frac{1}{2}^-$ state at 0.32 MeV. This experiment has been recently done at GANIL [42] as an initiative of studying the properties of low-lying states in exotic nuclei. We use Eq. (47) with $B(\mathrm{E1}) = 0.116\ e^2\mathrm{fm}^2$ which is deduced from the lifetime measurement by

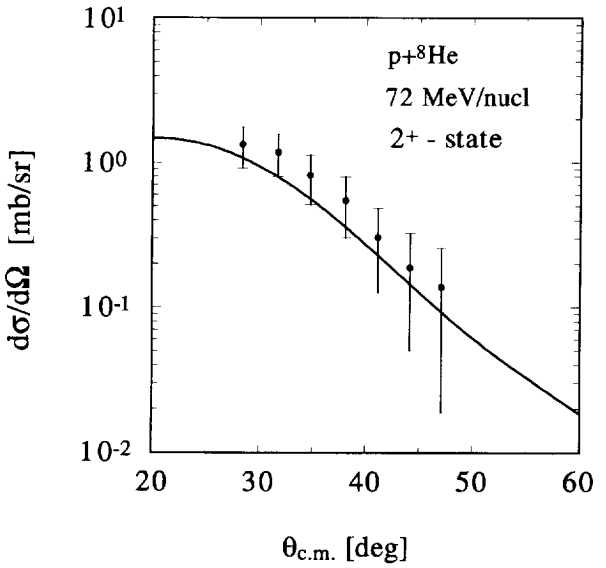

Fig. 11. Excitation cross section of the 2^+ state ($E_x = 3.57$ MeV) in ^{8}He by protons with 72 MeV. The data points are from Ref. [5]. The solid curve is obtained by using the "$t\rho\rho$" potential for p + ^{8}He and the deformed-potential model for the excitation, with $\beta_2 = 0.32$.

Millener et al. [43]. We obtain the solid curve shown in Fig. 12. The Coulomb cross section is peaked at very forward angles, as expected. The angular-integrated cross section is equal to 210 mb. We omit the nuclear contribution which is very small,

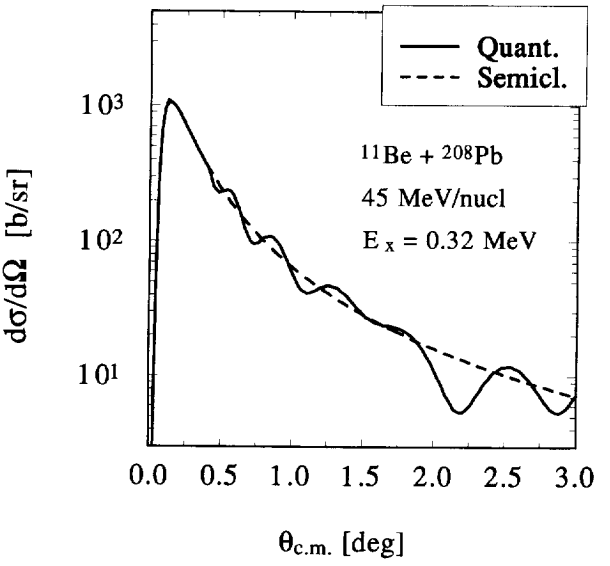

Fig. 12. Coulomb-excitation cross section of the $\frac{1}{2}^-$ state at 320 keV in ^{11}Be incident at 45 MeV/nucleon on a lead target. The solid curve uses Eqs. (47)–(49), with the eikonal phase calculated with the "$t\rho\rho$" approximation. The dashed curve is a semiclassical calculation using Eqs. (52), (53).

$\sigma_N = 12$ mb, and only important for large scattering angles. The cross section presents a wiggling at large scattering angles, characteristic of diffraction patterns in inelastic scattering. It is instructive to compare this result with a semiclassical calculation, based on Rutherford orbits for the trajectory of the nuclei and time-dependent perturbation theory [44]. In this case, the excitation cross section is given by

$$\frac{d\sigma}{d\Omega}(E_x) = \frac{16}{9\hbar c}\pi^3 B(E1, E_x)\frac{dn_{E1}}{d\Omega}, \tag{52}$$

where the equivalent photon numbers $dn_{E1}/d\Omega$ are given analytically by

$$\frac{dn_{E1}}{d\Omega_a} = \frac{Z_A^2\alpha}{4\pi^2}\left(\frac{c}{v}\right)^2 \epsilon^4 \zeta^2 \, e^{-\pi\zeta}\left(\frac{1}{\gamma^2}\frac{\epsilon^2-1}{\epsilon^2}\left[K_{i\zeta}(\epsilon\zeta)\right]^2 + \left[K'_{i\zeta}(\epsilon\zeta)\right]^2\right), \tag{53}$$

where $\epsilon = 1/\sin(\theta/2)$, $\alpha = \frac{1}{137}$, $\zeta = E_x a_0/\gamma\hbar v$, with $a_0 = Z_a Z_A e^2/2E_{lab}$.

Using the above expression for $dn_{E1}/d\Omega_a$ we obtain the dashed curve in Fig. 12 for the same reaction. One observes that the quantum result does not deviate from the semiclassical result appreciably. The good agreement especially at lower angles is quite satisfactory. This shows that strong absorption is not relevant for the scattering at low angles. The peak at small angles is a consequence of the adiabaticity condition. For $\zeta \gg 1$ ($\theta_a \ll 0.2°$) the Coulomb field is too weak to provide the necessary excitation energy. For $\zeta \ll 1$ ($\theta_a \gg 0.2°$) the Coulomb field is too strong and privileges the excitation of the projectile to higher energy states. Therefore, the cross section at a fixed relative energy of the fragments in the final channel has a peak at the optimal scattering angle corresponding to that energy. For the case above this angle is about 0.2°.

7. Conclusions

We have studied the applicability of simple concepts from scattering theory for intermediate-energy collisions as a tool to study the ground-state densities and the transition probabilities in reactions with radioactive nuclei. The eikonal approximation together with the "$t\rho\rho$" approximation yields simple and transparent formulas. This model gives very reasonable results for elastic-scattering cross sections at forward angles which can be used to test the ground-state densities of radioactive nuclei. The extended nuclear matter in exotic nuclei is manifest in the magnitude of the elastic cross sections as well as in the position of the first minimum as shown in Figs. 4–8.

We discussed also the model for the inelastic cross sections of nuclei to low-excited collective states and giant resonances. The model includes both the nuclear- and Coulomb-excitation processes. The transition densities from the ground state to continuum states have the characteristic of an extended tail at large distances from the nuclear center. In this article, we have presented a few cases of excited cross sections of nuclei and nucleon. Comparisons with the experimental data in Figs. 9–11 show that the folding model presented here is well suited to the study of inelastic excitations of not only stable but also radioactive beams. One specially interesting problem in unstable

nuclei would be a possible identification of soft multipole modes in such experiments. This could be accomplished by looking at the angular pattern of inelastic scattering since different multipolarities yield quite different patterns. This problem will be discussed in detail in a subsequent paper [45].

Acknowledgements

This work is supported financially by the Grant-in-Aid for Scientific Research on Priority Area (No. 06234212) by the Ministry of Education, Science and Culture, Japan.

References

[1] H. Toki, I. Tanihata and H. Kamitsubo, eds., Proc. Fourth Int. Conf. on Nucleus–nucleus collisions, Kanazawa, Japan, June 1991 (North-Holland, Amsterdam, 1992).
[2] I. Tanihata, H. Hamagaki, O. Hashimoto, Y. Shida, N. Yoshikawa, K. Sugimoto, O. Yamakawa, T. Kobayashi and N. Takahashi, Phys. Rev. Lett. 55 (1985) 2676.
[3] I. Tanihata, T. Kobayashi, O. Yamakawa, S. Shimoura, K. Ekuni, K. Sugimoto, N. Takahashi, T. Shimoda and H. Sato, Phys. Lett. B 206 (1988) 592;
I. Tanihata, private communication.
[4] C.-B. Moon et al., Phys. Lett. B 297 (1992) 39.
[5] A.A. Korsheninnikov et al., Phys. Lett. B 316 (1993) 38.
[6] J.J. Kolata et al., Phys. Rev. Lett. 69 (1992) 2631.
[7] M. Zahar et al., Phys. Rev. C 49 (1994) 1540.
[8] N. Takigawa, M. Ueda, M. Kuratani and H. Sagawa, Phys. Lett. B 288 (1992) 244.
[9] K. Ieki et al., Phys. Rev. Lett. 70 (1993) 6;
D. Sackett et al., Phys. Rev. C 48 (1993) 118;
T. Shimoura et al., Phys. Lett., in press.
[10] T. Nakamura et al., Phys. Lett. B 331 (1994) 296;
H. Sagawa et al., Z. Phys., in press.
[11] C.A. Bertulani and H. Sagawa, Phys. Lett. B 300 (1993) 205.
[12] M.S. Hussein, R.A. Rego and C.A. Bertulani, Phys. Reports 201 (1991) 279.
[13] S.M. Lenzi, A. Vitturi and F. Zardi, Phys. Rev. C 38 (1988) 2086; C 40 (1989) 2114; C 42 (1990) 2079; Nucl. Phys. A 536 (1992) 168.
[14] R.J. Glauber, High-energy collisions theory, Lectures in theoretical physics (Interscience, New York, 1959) p. 315.
[15] G. Fäldt, Phys. Rev. D 2 (1970) 846.
[16] A. Vitturi and F. Zardi, Phys. Rev. C 36 (1987) 1404.
[17] L. Ray, Phys. Rev. C 20 (1979) 1857.
[18] D. Vautherin and D.M. Brink, Phys. Rev. C 5 (1972) 626;
M. Beiner, H. Flocard, Nguyen van Giai and P. Quentin, Nucl. Phys. A 238 (1975) 29.
[19] P.G. Hansen and B. Johnson, Europhys. Lett. 4 (1987) 409.
[20] G.F. Bertsch, B.A. Brown and H. Sagawa, Phys. Rev. C 39 (1989) 1154.
[21] B.A. Brown, Nucl. Phys. A 522 (1991) 221c.
[22] G. Audi and A.H. Wapstra, Nucl. Phys. A 565 (1993) 1.
[23] C. Mahaux, P.F. Bortignon, R.A. Broglia and C.H. Dasso, Phys. Reports 120 (1985) 1.
[24] I. Hamamoto and P. Siemens, Nucl. Phys. A 269 (1976) 199.
[25] V. Bernard and Nguyen van Giai, Nucl. Phys. A 348 (1980) 75.
Z.Y. Ma and J. Wambach, Nucl. Phys. A 402 (1983) 275.

[26] H. Sagawa, Phys. Lett. B 286 (1992) 7.
[27] Nguyen van Giai and H. Sagawa, Phys. Lett. B 106 (1981) 379.
[28] B.A. Brown, C.R. Bronk and P.E. Hodgson, J. of Phys. G 10 (1984) 1683.
[29] H. De Vries, C.W. De Jager and C. De Vries, At. Data Nucl. Data Tables 36 (1987) 495.
[30] J. Barrette et al., Phys. Lett. B 209 (1988) 182.
[31] J. Berger et al., Nucl. Phys. A 338 (1980) 421.
[32] W. Czyz and L.C. Maximon, Ann. Phys. 52 (1969) 59.
[33] M. Buenerd et al., Phys. Rev. C 26 (1982) 1299.
[34] M.H. Macfarlane and S.C. Pieper, PTOLEMY, a program for heavy-ion direct-reaction calculations, Argonne National Laboratory report ANL-76-11 (1978), unpublished.
[35] N. Takigawa, M. Kurutani and H. Sagawa, Phys. Rev. C 47 (1993) R2470.
[36] C.A. Bertulani, L.F. Canto and M.S. Hussein, Phys. Reports 226 (1993) 281.
[37] G.R. Satchler, Nucl. Phys. A 472 (1987) 215.
[38] L.J. Tassie, Aust. J. Phys. 9 (1956) 407.
[39] C.A. Bertulani and A.M. Nathan, Nucl. Phys. A 554 (1993) 158.
[40] H.P. Morsch et al., Phys. Rev. Lett. 69 (1992) 1336.
[41] R.W. Berard et al., Phys. Lett. B 47 (1973) 355.
[42] P.G. Hansen, private communication.
[43] Millener et al., Phys. Rev. C 28 (1983) 497.
[44] C.A. Bertulani and G. Baur, Phys. Reports 163 (1988) 299.
[45] H. Sagawa and C.A. Bertulani, (1995), to be published.